An experimental study of the explosion generated by a pressurized sphere

By D. W. BOYER
Institute of Aerophysics, University of Toronto, Toronto, Canada*

(Received 22 December 1959 and in revised form 16 August 1960)

An experimental investigation of the explosions of 2 in. diameter glass spheres under high internal pressure has been made. The spheres were initially filled with air or helium at 400 and 326 p.s.i., respectively, and were exploded in air at atmospheric pressure. Experiments on the simulation of high-altitude explosions are also described. Schlieren and spark shadowgraph records of explosion phenomena, and pressure records of the reflexion of the spherical shock wave at various radii, are presented.

An account of some initial experiments on the implosion of 5 in. diameter glass spheres is given. The results were not very satisfactory because of the failure of the spheres to shatter in a desirable manner while under an external pressure of 65 p.s.i.

Numerical solutions to the air and helium sphere explosions are described and the experimental wave phenomena are shown to be in good quantitative agreement with the theoretical predictions, in that they exhibit all the main features that were predicted and are modified only by the physical limitations of the glass diaphragm. A formation process is associated with the spherical shock waves in practice, resulting in initial shock velocities which are lower than the theoretical values.

1. Introduction

The gas-dynamics of the spherical blast in air has attacted considerable attention over the past decade. Interest centred initially on similarity solutions to the hypothetical mass-less or point-source explosion in an ideal gas (von Neumann 1944; Taylor 1950*a*; Latter 1955) to describe the motion of a strong spherical shock (or blast) wave generated by the sudden release of a large amount of energy, initially in an infinitely concentrated form, under the assumption that the form of the profiles of pressure p, density ρ, temperature T, and velocity u, from the origin to the shock radius, are invariant with time. Similarity solutions may also be derived for plane (Harris 1956) or cylindrical (Lin 1954) flows. The applicability of similarity analyses, however, is limited to strong waves as the similarity assumptions are consistent only with the strong-shock form of the Rankine–Hugoniot condition (i.e. shock density ratio = 6 for a specific heat ratio $\gamma = 1{\cdot}4$).

In order that blast-wave calculations may be extended down to lower shock-

* Now at Cornell Aeronautical Laboratory, Inc., Buffalo, N.Y., U.S.A.

pressure ratios, the usual form of the Rankine–Hugoniot condition must be incorporated as a non-stationary shock boundary condition in the non-linear partial differential equations. However, no integrable solution of these equations has yet been found and one must resort to numerical methods. Two numerical solutions to the point-source explosion in an ideal gas have been reported (Goldstine & von Neumann 1955; Brode 1955*a*). In view of the assumption of constant specific heat, however, the above point-source solutions are in error for very strong shock waves where high-temperature effects become appreciable. However, in a later paper (Brode 1956), the thermal and caloric equations for an imperfect gas were incorporated in a numerical solution of the point-source explosion in real air.

Recently, particular attention has been given to the flow phenomena accompanying an ordinary (finite source) explosion; the explosions produced, for example, by the detonation of shaped charges of high explosive, the vaporization of wires by high-energy electrical discharges, or, as in the case of present interest, by the sudden release of high-pressure gas spheres (Brode 1955*b*).

The wave phenomena following the sudden shattering of 2 in. diameter glass spheres, initially filled with air or helium at high pressure, have been studied by optical methods in the UTIA shock sphere. This investigation is an extension of previous work on spherical flows which was undertaken in collaboration with H. L. Brode of the Rand Corporation, who performed detailed numerical calculations for the conditions pertinent to the present experimental work (Boyer, Brode, Glass & Hall 1958). The principal optical records were radius-time plane schlieren photographs. Spark shadowgraph pictures are also presented in addition to pressure records obtained from a quartz transducer placed normal to the flow at various radii.

The present paper describes these experiments and discusses the comparison of the helium and air sphere explosions with their numerical solutions. The results of some initial experiments on implosions are also described.

2. Theoretical résumé

The equations of motion for spherical symmetry, neglecting viscosity and heat condition, are written in Lagrangian form, choosing as independent variables the time t and the initial radial position r_i of a fluid element. For convenience, the latter variable is replaced by a mass variable X defined by $X = \frac{1}{3}\rho_i r_i^3$, where ρ_i is the initial gas density in the fluid element at r_i.

In order that the equations may be generally applicable to any initial total energy E and any pre-shock conditions p_1, ρ_1, a_1, where a is the sound speed, they are made non-dimensional by expressing the dependent variables in terms of some standard initial values. Accordingly, we define

$$\pi = p/p_0, \quad \eta = \rho/\rho_0, \quad \beta = u/a_0, \quad \theta = T/T_0, \tag{1}$$

where the initial values are those corresponding to $p_0 = 14{\cdot}7$ p.s.i. and $T_0 = 0\,^\circ\mathrm{C}$. The quantities p_0, ρ_0 and a_0 have been used for convenience and are not to be confused with the actual atmospheric conditions p_1, ρ_1 and a_1 which are necessary

for actual scaling purposes. The independent variables are made non-dimensional in terms of the initial energy:

$$\tau = a_0 t/\epsilon, \quad x = X/\rho_0 \epsilon^3, \quad \lambda = r/\epsilon, \tag{2}$$

where

$$\epsilon^3 = E/p_1, \tag{3}$$

and

$$E = \tfrac{4}{3}\pi r_i^3 p_4/(\gamma - 1), \tag{4}$$

the total energy initially in the sphere (region 4).

In order to avoid the difficulties associated with the treatment of shock discontinuities in the numerical calculations, Brode employed the artificial viscosity technique due to von Neumann & Richtmyer (1950). Discussions on the required form for the artificial viscosity in calculations of this sort have been described elsewhere (Brode 1955*a*; Latter 1955). The form of the artificial viscosity ζ used is

$$\zeta = \frac{9\gamma(\gamma+1)}{4}\left(\frac{M}{3\pi}\right)^2 \rho(\Delta x)^2 \frac{\partial u}{\partial x}\left(\frac{\partial u}{\partial x} - \left|\frac{\partial u}{\partial x}\right|\right), \tag{5}$$

where Δx is the spacing of the integration network and M is the number of spatial zones in the shock front. This form for ζ satisfies the requirement that the artificial viscosity contributes nothing outside the shock transition region, i.e. that the rest of the flow field remains unaltered, since for $\partial u/\partial x$ positive, or zero, $\zeta = 0$ and the artificial viscosity contributed nothing, either in the initial rapid expansion region where the positive velocity gradient is large, or in the contact front. Furthermore, because of the small grid-size term Δx, ζ becomes appreciable only in regions of large negative $\partial u/\partial x$, i.e. in the shock transition region.

The dimensionless parameters (1) and (2) are then incorporated into the Lagrangian equations of motion. Since the artificial viscosity (5) has the dimensions of pressure, it is non-dimensionalized ($q = \zeta/p_0$) and included in the equations with the fluid pressure term. We then obtain

$$\frac{1}{\eta} = \lambda^2 \frac{\partial \lambda}{\partial x} \quad \text{(mass)}, \tag{6}$$

$$\frac{\partial \beta}{\partial \tau} = -\frac{\lambda^2}{\gamma}\frac{\partial}{\partial x}(\pi + q) \quad \text{(momentum)}. \tag{7}$$

Also, from the condition that the entropy is a constant along a given particle path (particle isentropic), the following applies:

$$\frac{\partial \pi}{\partial \tau} = \frac{1}{\eta}\frac{\partial \eta}{\partial \tau}[\gamma\pi + (\gamma - 1)q] \quad \text{(entropy)}, \tag{8}$$

and

$$\beta = \frac{\partial \lambda}{\partial \tau} \quad \text{(velocity)}. \tag{9}$$

It is seen from the expression (4) for E that for a particular gas and gas pressure (γ and p_4) in the sphere, the initial energy density (energy/unit volume) is fixed. The situation is analogous to that of a charge of a particular explosive, and an increase in r_i, the initial sphere radius, is equivalent to an increase in the size of the charge. A change in either p_4 or γ, however, alters the initial energy density and is equivalent to a change from one type of explosive to another.

It was first shown empirically by Cranz (Schardin 1954) that in the explosion of two different sizes of charge of a particular explosive, in identical atmospheric conditions, the same blast pressures occur at shock radii r_s which are related to the initial explosive energies by

$$\frac{r_{s(A)}}{r_{s(B)}} = \left(\frac{E_A}{E_B}\right)^{\frac{1}{3}}, \quad \text{or, from (3),} \quad \frac{r_{s(A)}}{r_{s(B)}} = \frac{\epsilon_{(A)}}{\epsilon_{(B)}}. \tag{10}$$

This scaling law may be investigated by experiments on the explosion of spheres initially at the same pressure but having different initial radii. Cranz's principle is automatically taken into account in the present analysis by using ϵ as a non-dimensionalizing quantity for the radial distance and the time. Furthermore, for a given initial sphere size, it is also possible to simulate explosions at arbitrary altitudes (altitude scaling) by scaling the energy density p_4 in the sphere by the same factor as the external pressure p_1.

Brode solved the non-linear partial differential equations (6) to (9) by numerically integrating in a step-by-step manner a set of stable approximate difference equations (Brode 1956), using a real-gas equation of state for air. The solutions to the air and helium sphere problems are calculated for the following initial conditions:

Air/Air	$p_4 = 326$ p.s.i.,	$\pi = 22{\cdot}1768$,
	$p_1 = 15$ p.s.i.,	$\pi_i = 1{\cdot}0204$,
	$T_1 = 299$ °K,	$\theta_i = 1{\cdot}0952$,
	$\epsilon = 6{\cdot}12 r_i$,	$\lambda = 0{\cdot}163 r/r_i$,
	$r = 6\lambda$ in.,	$t = 460\tau$ μsec.
He/Air	$p_4 = 263{\cdot}7$ p.s.i.,	$\pi = 17{\cdot}9387$,
	$p_1 = 14{\cdot}45$ p.s.i.,	$\pi_i = 0{\cdot}9830$,
	$T_1 = 300{\cdot}7$ °K,	$\theta_i = 1{\cdot}1014$,
	$\epsilon = 4{\cdot}83 r_i$,	$\lambda = 0{\cdot}207 r/r_i$,
	$r = 4{\cdot}71\lambda$ in.,	$t = 360\tau$ μsec.

The notation Air/Air or He/Air denotes the case of a pressurized air or helium sphere, respectively, exploded in air (region 1).

3. Numerical results and discussion

3.1. *The overpressures*

The calculated decline in shock overpressure ΔP_s with shock radius λ_s is shown in figure 1 for the point-source blast in air and in an ideal gas. The shock overpressure, $\Delta P_s = \pi_s - \pi_i$, refers to the pressure in atmospheres, immediately behind the shock wave, in excess of the initial or pre-shock pressure, and the shock radius, $\lambda_s = r_s/\epsilon$, is in the energy-reduced dimensionless units defined previously. For the real gas case, it is seen that the blast overpressures are lower, at any radius, than those for the point-source explosion in an ideal gas since a further amount of the available energy must now go into the dissociation and ionization of the high-temperature air in the real gas case.

For comparison, the corresponding curves for the blasts from the air and helium spheres are shown on the same figure. Also included is the shock-over-

pressure curve for the blast from a spherical charge of TNT (Brode 1959). The initial behaviour of the gas sphere and TNT curves is quite different from that of the point-source curves because of the more complex gas dynamics associated with any finite-source explosion (new rarefaction and shock-wave phenomena, shock wave–contact surface interactions, etc.). However, at increasing distances from a finite-source explosion, the resulting blast wave will appear more and more like that from a point source. It has been shown (Brode 1955*a*, *b*) that the blast from an initially static, high-pressure sphere will assume the general shape and

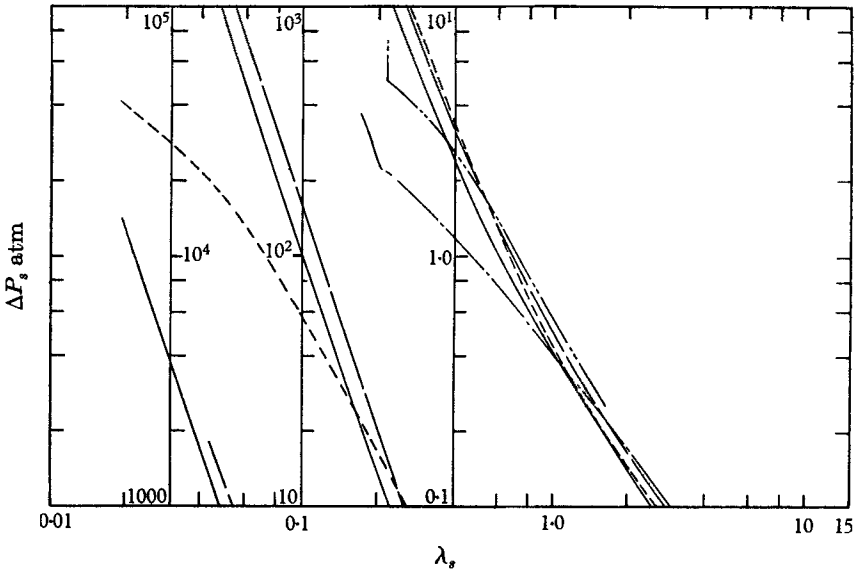

FIGURE 1. Shock overpressure ($\Delta P_s = \pi_s - \pi_i$) versus shock radius ($\lambda_s = r_s/\epsilon$) for various explosions. Point source in air (real gas), ——; point source in ideal gas, — —; bare sphere of TNT, – – – –; helium sphere (264 p.s.i.), — — — —; air sphere (326 p.s.i.), — — —.

values of the point-source blast after the shock wave has engulfed a mass of air approximately equal to 10 times the initial mass in the sphere. The shock overpressure in the blast from a source of large initial mass may therefore fall to quite low values before the point-source solution is reached. Such is the case for the blasts from the present air and helium spheres, which initially contained gas at high density and low (room) temperature. The present curves do not reach point-source values until quite low overpressures, 2 atm in the case of the helium sphere and 0·4 atm for the air sphere. These shock overpressures correspond to shock radii of 2·6 and 6 in. respectively, at which point the shock has engulfed a mass of air equal to 6·8 and 9·9 times the initial mass in each sphere. Because of its lower mass, the approach to the point-source curve is more rapid in the helium case.

For the same initial pressure ratio and sphere size, the total energy initially in an air or helium sphere may, from (4), be written as

$$E = \text{constant}\left(\frac{1}{\gamma - 1}\right).$$

Consequently, when scaling is possible, i.e. when the blast overpressures have reached point-source values, the air sphere is more efficient as a blast producer because it contains 5/3 as much energy as the helium sphere under the same initial pressure ratio. Actually, in the present case, the air sphere contains twice the amount of energy in the helium sphere because of the higher initial pressure in the air case.

3.2. *The wave systems and pressure profiles*

The theoretical distance–time (r, t) wave diagram for the air-sphere burst is shown in figure 2. At $t = 0$, a 2 in. diameter sphere of air at a pressure of 326 p.s.i. and a temperature of 299 °K (region 4) is suddenly released into atmospheric air at the same temperature (region 1). Theoretical profiles of the pressure ratio π as a function of the reduced radius λ at various times during the air-sphere explosion are shown in figure 4. The times after release are given in microseconds and the position of the contact surface is indicated by a bar on the curves.

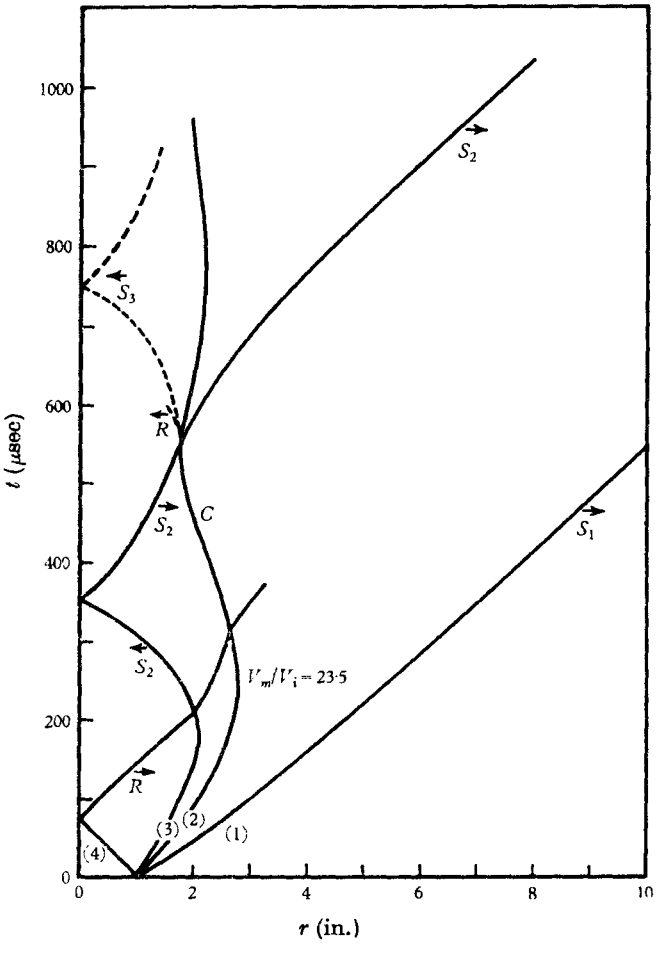

FIGURE 2. Theoretical wave system for the explosion of a 2 in. diameter sphere of air initially at 326 p.s.i.

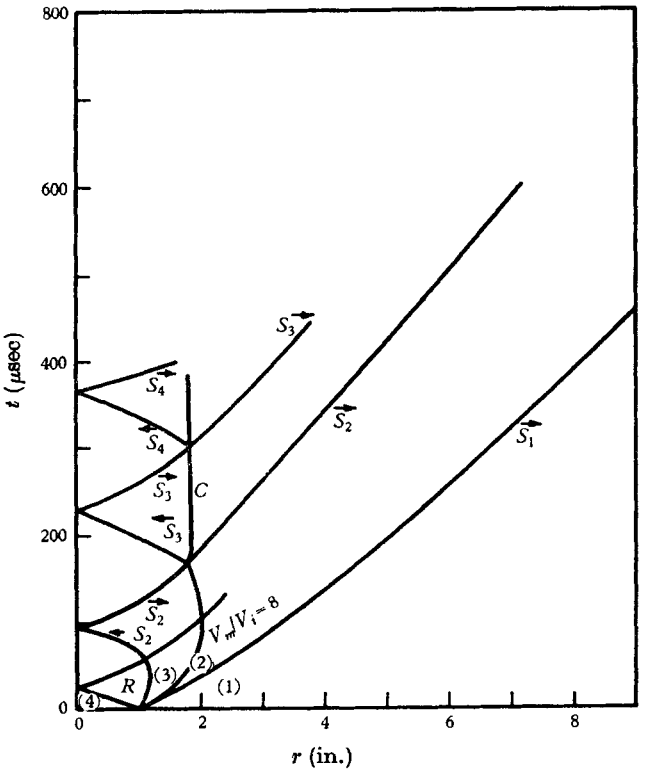

FIGURE 3. Theoretical wave system for the explosion of a 2 in. diameter sphere of helium initially at 264 p.s.i.

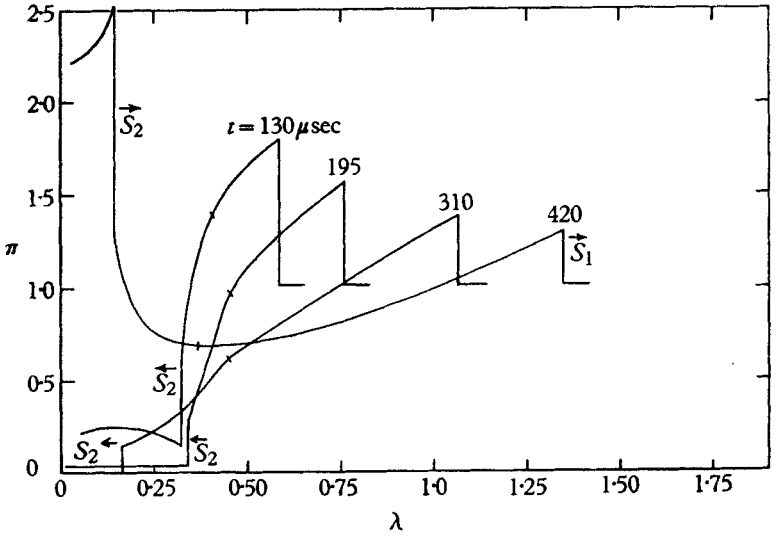

FIGURE 4. Pressure ratio ($\pi = p/p_0$) versus radius ($\lambda = r/c$) at indicated times t in the explosion of a sphere of air initially at 326 p.s.i. Bars denote position of the contact surface.

Immediately after release (figure 2), a spherical shock wave $\vec{S}_1$ is generated and moves out into the surrounding air. The compressed sphere gas is expanded through a spherical rarefaction wave $\overleftarrow{R}$ and a contact front C separates the expanded sphere gas from the air compressed by the shock. However, because of the three-dimensionality of the flow, no steady-state regions exist following a sudden spherical expansion, and the contact front and all discrete wave elements, with the exception of the head of the rarefaction wave, are curved in the distance–time plane.

Figure 4 shows that the pressure is a maximum immediately behind the shock wave and that it falls off continuously with increasing distances behind the shock front. Qualitatively, after a spherical shock wave has passed, the pressure at a particular radius decreases with time, resulting in the generation of expansion waves which move throughout the entire flow field. Those generated from expanding fluid elements close behind the shock wave, are able to overtake the shock and so cause it to attentuate.

Since the mass of gas in a particular fluid element must remain constant, it follows that as the fluid elements of the high-pressure gas pass through a spherical rarefaction wave, they must expand to lower pressures than those reached through an equivalent one-dimensional expansion.

As a result of these pressure variations, an inward facing, second shock wave $\overleftarrow{S}_2$ exists in the spherical flow field. Although no mechanism is postulated for the development of this shock wave, its formation must be a consequence of the greater freedom for expansion in this type of flow. It is, in fact, a characteristic of cylindrical and spherical flows in general. The second shock wave has its origin at the tail of the rarefaction wave and develops there at an early time as the flow begins to experience a departure from a one-dimensional type of expansion. Although S_2 is an inward facing wave, it is initially quite weak and is therefore swept outwards because of the high expansion velocity (figure 4). However, as its strength is continually increasing, it soon comes to rest and then moves in to implode on the origin as shown in the last three curves of figure 4.

The contact surface initially moves outwards behind the main shock wave but with a continually decreasing velocity. After 220 μsec, the front ceases its outward motion altogether and begins to move in towards the origin again, following the inward motion of the gas induced by the rapidly imploding second shock wave. The velocity of the inward moving gas increases from the contact front to a maximum just behind S_2. The second shock itself, however, is moving into an expanding region of flow, the outward expansion velocity being a maximum immediately in front of S_2.

The path taken by the contact front is indicative of the paths taken by fluid elements behind the main shock wave, i.e. the flow velocities behind a spherical shock wave will exhibit a negative phase in which particles that have been set into outward motion by the shock will gradually come to rest and then move back towards their initial positions. (A negative phase of velocity refers to the fact that the particle velocity is directed towards the sphere centre; a negative phase of overpressure refers to the fact that the pressure has fallen below the initial or pre-shock pressure.)

After implosion, the second shock wave moves out again, interacts with the contact surface, and is transmitted through the front. This shock, however, does not overtake the main shock S_1 in the present Air/Air problem as it emerges from the contact front behind the maximum of the negative velocity phase of the main shock. Furthermore, in interacting with the contact surface, the second shock wave passes from cold dense air to hotter, more rarefied air and as a result, a rarefaction wave is reflected back towards the origin from the point of interaction.

Following this second inward rarefaction wave is an inward-facing third shock wave S_3 as the situation is again similar to that requiring the formation of S_2.

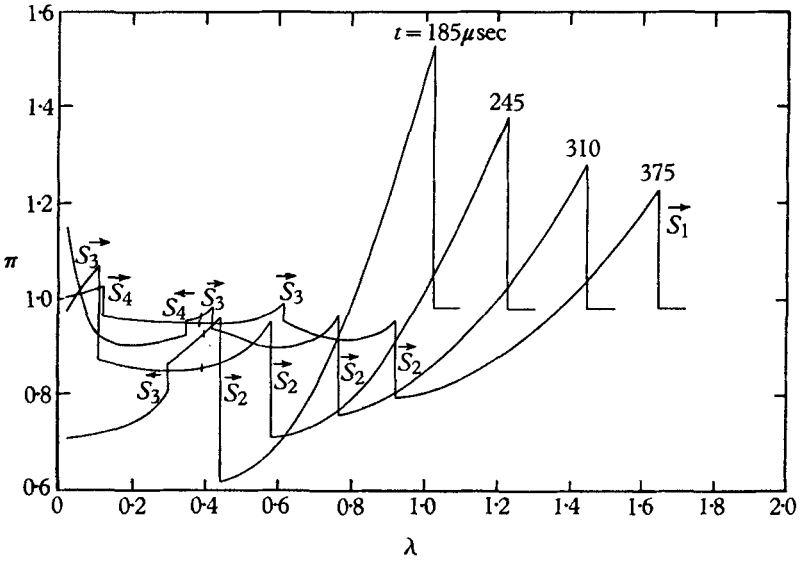

FIGURE 5. Pressure ratio ($\pi = p/p_0$) versus radius ($\lambda = r/\epsilon$) at indicated times t in the explosion of a sphere of helium initially at 264 p.s.i.

In the present case, however, the third shock is so weak, and occurs so late in the problem that it is difficult to detect in the numerical solution. Consequently, the indicated path for S_3 in figure 2 is only approximate. These events are repeated as further reflexions and refractions occur at the contact surface. The path of the reflected head of the initial rarefaction wave is also shown in the figure. Further reflexions and refractions take place as this wave passes through the second shock wave and the contact surface, and it is evident that the flow in the interior regions of the Air/Air problem becomes quite complex.

The theoretical distance–time (r, t)-wave system following the sudden release of a 2 in. diameter sphere of helium, initially at 264 p.s.i. and 300·7 °K is shown in figure 3. Theoretical profiles of the pressure ratio π as a function of the reduced radius λ at selected times during the helium-sphere explosion are shown in figure 5 and will be referred to in the discussion of the wave diagram of figure 3.

The initial development of the flow is the same as that previously described for the Air/Air case. In detail, however, the helium problem is quite different.

In spite of the lower initial pressure ratio, the main shock wave S_1 is initially stronger than that in the air problem because helium has a higher sound speed and is a more efficient driver as in the shock tube case. Because of this higher sound speed, a speed almost three times that in air at the present initial temperatures, the expansion of the high-pressure helium is considerably more rapid that the air expansion. As a consequence, the second shock wave in the helium case implodes on the sphere centre in almost a quarter of the time taken in the air case (94 μsec compared with 350 μsec), after being swept out for a shorter time (41 μsec compared with 173 μsec) and to a smaller maximum radius (1·2 in. compared with 2·1 in.).

The main difference between the helium and air problems, however, is in the nature of the interior flow between the origin and the contact surface. The second shock wave moves against the gas flow both during the implosion and after reflexion from the centre of the sphere and is then transmitted through the contact surface to travel outward behind the main shock. As in the air problem, this shock wave lies behind the maximum of the negative velocity phase of S_1 and therefore does not overtake the main shock wave. The same is true, incidentally, in the TNT case (Brode 1959). The wave system for the helium case is, in fact, very similar to that calculated for the TNT explosion. However, for a similar problem in which the sphere of gas is initially at a very high temperature, the second shock wave moves out earlier and is able to overtake and reinforce the main shock wave (Brode 1955*b*).

On traversing the helium–air interface, S_2 encounters a hotter denser gas and as a result a third shock wave S_3 is reflected from the interface and travels back towards the centre of the sphere (figure 5, 185 μsec). At this stage the contact surface is essentially stationary as distinct from the oscillatory motion of the air-sphere interface. After reflexion from the centre of the sphere, S_3 undergoes a further intersection with the contact surface generating a fourth shock S_4, which moves inward through the helium, and the third shock is transmitted to follow S_2 (figure 5, 310 μsec). The helium interior is therefore repeatedly traversed by shock waves as further interactions occur.

3.3. *The temperature profiles*

Theoretical space plots of the temperature as a function of the radius for the air-sphere problem are shown in figures 6 and 7. Temperatures have been given in °K and the radii in inches, and each curve is identified by the elapsed time in microseconds after release. The early development of the flow over the first 40 μsec is shown in figure 6 and the contact surface is now clearly indicated by the temperature discontinuity there.

Perhaps the most noticeable feature in this figure is the increase in temperature behind the main shock wave. When a spherical shock wave passes through the air, the entropy of the air is increased by an amount which depends upon the strength of the shock wave. However, since a spherical shock wave attenuates with increasing distance from its source, the entropy increase imparted to the air diminishes with increasing shock radius. The air is therefore left in a state in which the entropy decreases radially.

In the previous discussion of the (r, t)-wave diagrams, it was shown that the pressure of fluid elements set in motion by the shock wave decreases as the elements move out to larger radii (greater volumes). In expanding, the temperature of these elements decreases. This cooling is therefore in opposition to the temperature increase of each fluid element due to entropy addition imparted

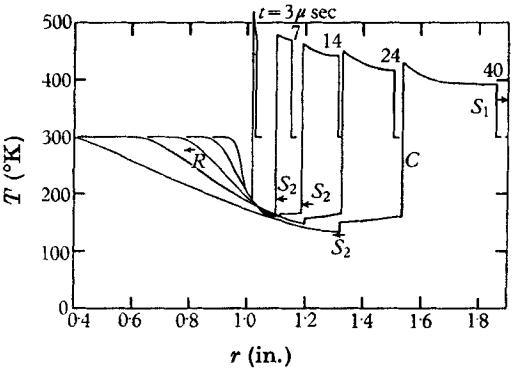

FIGURE 6. Temperature T versus radius r at indicated times t in the explosion of a sphere of air initially at 326 p.s.i.

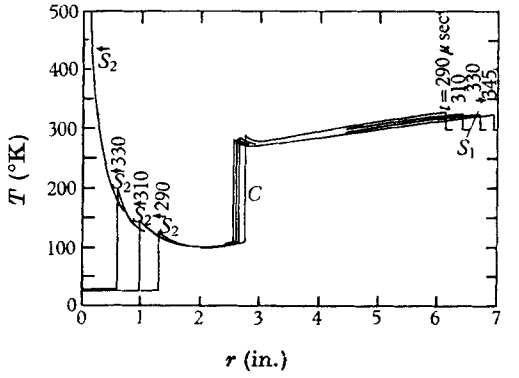

FIGURE 7. Temperature T versus radius r at indicated times t in the explosion of a sphere of air initially at 326 p.s.i.

by the shock. When the shock waves are reasonably strong, however (figure 6), the effect of entropy increase is dominant and the curves show an increase in temperature with distance behind the shock. However, at later times when the shock has decreased in strength (figure 7) the entropy increase becomes insignificant, being of only third order in the shock strength for weak shocks, and the temperature decrease due to expansion becomes dominant.

Temperatures at times during the implosion of S_2 are shown in figure 7. The solution indicates that the initial expansion lowers the temperature in front of the imploding shock wave to about 25 °K. Actually, of course, the component gases of air would be solid at this temperature. The temperature after expansion in the corresponding shock-tube problem is 180 °K. After S_2 has passed, the air between S_2 and the contact surface remains at about 100 °K. Temperature profiles

within the first 20 μsec in the helium-sphere explosion are similar to those discussed above for early times in the air problem and show a temperature increase with distance behind the shock front. The temperature attains higher values in this case, however, because of the stronger initial shock. At later times, temperature profiles in the helium case reflect the more complex shock history in the helium interior.

A noticeable feature in the air and helium-sphere solutions is the fact that temperatures near the origin remain quite high after the implosion of S_2. The repeated compression of the sphere gas by the implosion of shock waves arising from shock-contact surface interactions, is responsible for the change from the initial isothermal temperature distribution. The temperature increases at points progressively closer to the origin as the strength of the imploding shock wave increases (figure 7). This type of temperature distribution at the origin is characteristic of the point-source case. The present distribution would be altered, however, by the inclusion of heat conduction in the analysis.

Further theoretical profiles for the present Air/Air and He/Air problems have been reported previously (Boyer *et al.* 1958; Boyer 1959). These include plots of the temporal and spatial variation of the density and particle velocity, the variation of the values of these quantities immediately behind the shock front with shock radius, and plots of the durations of the positive phase of shock overpressure, velocity and impulse.

4. Experimental equipment

The experiments were conducted in the 3 ft. diameter shock sphere at the Institute of Aerophysics. Pressure and vacuum lines to the shock sphere are controlled from a console and enable the shock sphere to be either evacuated or pressurized and provide for up to two glass spheres to be independently evacuated or pressurized with the same or different gases. The glass spheres (soda-lime and Pyrex) were hand blown to the required diameter and fitted with a 3 in. stem of 7 mm glass tubing. The glass spheres (without stems) weighed from 15 to 18 g each and had a nominal wall thickness from about 0·030 to 0·040 in. The stems were cemented (Hysol) into 4 in. lengths of $\frac{1}{4}$ in. pipe and the prepared sphere was installed at the centre of the shock sphere. The glass spheres were shattered by means of a solenoid-actuated, spring-loaded mallet, the operation of which was synchronized with the shutter of a rotating drum camera used in recording the schlieren (r, t)-plane records. An SLM PZ-6 quartz pressure transducer was mounted in a special holder in the end of a steel tube which passed through a port in the side of the shock sphere and was used to obtain pressure records of the flow at various radii.

5. Experimental procedure

5.1. *Scope of the experimental work*

In the course of the present experimental programme, spherical flows were initiated by the sudden shattering of glass spheres initially in a state of high tensile or compressive stress as a result of a pressure differential. The experi-

mental study consisted of two parts. The first and major portion of the work was concerned with the explosion of 2 in. diameter glass spheres, initially filled with air at 400 p.s.i. or helium at 326 p.s.i. The second part of the work was concerned with the implosion of 5 in. diameter glass spheres, initially evacuated to a pressure of 300 mm Hg while under an external (air) pressure of 65 p.s.i. Schlieren radius–time plane photographs of the flow from the exploding air and helium spheres were obtained by using a 12 in. diameter schlieren optical system in conjunction with a rotating drum camera. Measurement of the schlieren records enabled the velocities of all shock phenomena to be determined at various radii. The velocity of the glass fragments was also measured from the schlieren record of each explosion. Instantaneous spark shadowgraph pictures of the air and helium-sphere explosions were recorded at various times following the shattering of the spheres. A spark source was used in conjunction with one of the 12 in. diameter, 71·5 in. focal length parabolic schlieren mirrors to produce a parallel beam for direct shadowgraphs. The spark circuitry was so arranged that the spark was triggered, after a preset delay, by contact between the breaker mallet and a strip of aluminium foil glued to the base of the glass sphere.

The pressure history behind the reflected spherical shock wave was recorded at several radii in the air and helium-sphere explosions, including those on altitude scaling. An SLM PZ-6 quartz transducer was mounted normal to the flow and the transducer output was recorded on a Tektronix 545 oscilloscope. The pressure measurements served as a check on the wave-speed studies rather than a means of measuring pressure profiles at a given radius as a function of time since pressure measurements of this type require the use of small blast-type gauges. Such gauges were not available for these experiments. The SLM gauge was calibrated statically in an Ashcroft dead weight gauge tester. A dynamic calibration was also performed by mounting the gauge in the end-plate of a shock tube and comparing the measured pressure behind the reflected shock wave with that calculated from simple shock-tube theory for an incident shock wave of pressure ratio 4, for which viscous effects in the shock tube are negligible. These calibration procedures were in excellent agreement and showed a gauge sensitivity of 10 mV/p.s.i. for the selected pressure range of the instrument. The pressure records were obtained simultaneously with the schlieren records.

5.2. *Correction for the glass fragments*

Although the theoretical calculations were carried out for initial air and helium-sphere pressures of 326 and 264 p.s.i. respectively, the corresponding experimental pressures were 400 and 326 p.s.i. The higher initial pressures in the experimental case represent a correction for the kinetic energy possessed by the rapidly moving glass fragments, since the energy involved in glass motion represents a decrease in the total amount of energy available for the rest of the flow. The initial experimental work was therefore concerned with the measurement of the energy involved in the motion of the glass fragments. Schlieren records were obtained of a number of trial air and helium-sphere explosions at several initial sphere pressures. Since the mass of glass in each sphere (excludingthe stem) was known, the glass velocities obtained from the schlieren photographs enabled the

kinetic energies to be calculated. Differences between these energies and the initial energies in the spheres were compared with the corresponding energies assumed in the theoretical calculations. In this way it was possible to decide upon a value for the initial sphere pressure to be used in the air and helium explosions which would approximately account for the energy later taken up as kinetic energy by the moving glass fragments.

The glass kinetic energies were calculated subsequently from all the experimental runs and indicated that the initial pressures of 400 and 326 p.s.i. in the air and helium spheres, respectively, adequately accounted for the initial pressures of 326 and 264 p.s.i. used in the theoretical calculations. The average velocity of the glass fragments was 295 ft./sec in the 18 g air-sphere explosions, and 215 ft./sec in the 16 g helium-sphere explosions. In both cases, approximately 16 % of the initial energy appeared as kinetic energy of the glass fragments.

5.3. *Altitude scaling*

Some experiments on altitude scaling were performed in which pressurized air and helium spheres were exploded in air at reduced pressure. It was mentioned in § 2 that the non-dimensionalized equations are applicable to any pre-shock conditions (provided the initial pressures are not low enough for dissociation and ionization to occur). Consequently, it is seen from the expression for ϵ (equations (3) and (4)), where

$$\epsilon^3 = \tfrac{4}{3}\pi r_i^3 \frac{p_4}{(\gamma-1)p_1},$$

that, for a particular size of initial sphere (r_i), at standard temperatures, ϵ remains unaltered if the initial sphere density, or pressure (p_4), is changed by the same factor as the external pressure (p_1). The calculated solutions to the air and helium-sphere problems are, therefore, still applicable. Similarly, schlieren (r, t)-plane photographs of such scaled explosions should be quantitatively the same as those of the previous explosions in air at atmospheric pressure. Incidentally, in the case of a solid explosive, no such altitude scaling experiments are possible because of the fixed energy density of the charge.

A series of experiments was therefore performed in which glass spheres, initially pressurized with air or helium to 200 and 163 p.s.i. respectively, were exploded in air at a pressure of 0·5 atm (7·3 p.s.i.). This external pressure is equivalent to the atmospheric pressure at an altitude of 18,000 ft. In reducing the initial sphere pressures to half their previous values for these scaling experiments, the pressure correction for the energy of glass motion was automatically halved also. However, the kinetic energies were also calculated from these experiments and it was found that the glass took the same proportion of energy from the flow as in the unscaled explosions. The initial sphere pressures in these experiments were then satisfactory for scaling as required. The glass spheres were lighter (15 g) than those used in the unscaled explosions, and the average glass fragment velocities were smaller, 230 ft./sec in the air case and 150 ft./sec in the helium case.

6. Experimental results and discussion

6.1. *Shadowgraph records of the explosions*

Representative spark shadowgraph pictures of the explosion of the air spheres are shown in figures 8 (plate 1) and 9 (plate 2). The shadowgraphs were recorded from individual explosions at the indicated time delays after the mallet struck the sphere. A portion of the $\frac{1}{4}$ in. pipe which initially held the glass sphere appears at the top of each picture. The plunger of the solenoid-operated breaker is also visible. The fine wire appearing in each of these shadowgraphs is part of the spark circuitry which was triggered by contact between the aluminium foil and the grounded breaker mallet.

Figure 8 was recorded 300 μsec after the mallet struck the glass sphere. The shock wave is seen to be reasonably well formed, although there is still some non-uniformity in the curvature of the shock profile. Numerous compression waves may also be seen in the air behind the shock front. These experiments have shown that the spherical shock wave is not generated immediately, but is formed, as in the plane case, by the overtaking and coalescing of many compression fronts. The glass sphere has shattered though it still maintains a spherical shape and the sphere interior is completely masked by the glass fragments. These fragments will be seen to cause the complete obliteration of the early interior flow phenomena in the schlieren photographs. The turbulence in the escaping gas and the irregular profile of the interface are well illustrated in these shadowgraph pictures.

After 320 μsec (figure 9), the shock front is quite spherical, illustrating the stability of form exhibited by the main spherical shock wave in these experiments in smoothing out, or redistributing the non-uniformities in shock curvature at earlier times. The shock wave is diffracting around the pressure-gauge holder in this figure and the shock wave reflected from the face of the holder is moving back towards the exploding sphere. The small dark objects in the expanding sphere gas at the bottom of this spark picture are pieces of the strip of aluminium foil initially glued to the base of the sphere. During the equalization of the pressures behind the reflected and diffracted shock waves, a vortex is formed as the flow separates around the front edge of the gauge holder. This vortex then travels along the holder behind the diffracted shock wave. The developing vortex is just visible in this figure and weak disturbances may still be seen in the flow field between the interface and the shock front.

Unfortunately, because of the extreme irregularity of the contact front, caused by the presence of glass fragments in the escaping sphere gas, it was not possible to observe the effect of the deceleration of the contact region on the stability of the interface in the air and helium-sphere problems. This refers to the stability of the interface between two accelerated fluids of different densities. The stability condition derived for the plane case (Taylor 1950*b*) shows that the interface is stable (or unstable) if the acceleration is directed from the heavier to the lighter fluid (or vice versa). The corresponding problem for fluids in radial motion has been treated by Plesset (1954). Accordingly, since the density in the contact region in the Air/Air case is greater than that of the shocked air outside,

the decelerating interface in the air-sphere explosions should always be unstable. The helium–air interface, on the other hand, should be stable because of the slightly denser region outside the front. It may be shown, however, that under certain conditions (Plesset 1954) in the spherical problem, instability is also possible in the latter case.

6.2. *Schlieren records of the explosions*

A radial distance–time (r, t)-plane schlieren record of the flow during the explosion of a 2 in. diameter air sphere is shown in figure 10 (plate 3), together with an explanatory diagram. The initial sphere pressure in this case was only 326 p.s.i., the pressure assumed in the theoretical air calculations, and the figure has been included for purposes of schlieren photograph interpretation only. The record was taken during the initial series of explosion experiments in order to determine approximately what percentage of the energy assumed available for the flow in the theoretical calculations actually appeared as kinetic energy of the moving glass fragments. The radial distance and time scales indicated in the explanatory diagram of figure 10 apply to all the schlieren photographs.

Perhaps the most noticeable feature in this schlieren record is the excellent symmetry of the flow. The figure shows good quantitative agreement with the theoretical wave diagram for the Air/Air case (figure 2). The main spherical shock wave $\vec{S}_1$ is shown moving outwards, followed by the contact surface C, which quickly comes to rest and then moves in slightly towards the original sphere centre. The implosion of the second shock wave $\overleftarrow{S}_2$ is discernible in the photograph and its subsequent outward motion from the centre is seen quite clearly. No third shock wave was evident in any of the Air/Air schlieren records. The shock wave $\vec{S}_{1R}$ reflected off the pressure gauge is also seen moving back into the flow. Because of the decrease in outward flow velocity with increasing distance behind the shock front, $\vec{S}_{1R}$ is seen to accelerate as the velocity of the opposing flow decreases. The gauge in this case was located at a radius of 7 in. These reflected shocks will appear in most of the (r, t)-photographs since the schlieren records were taken in conjunction with the pressure measurements. The unbroken glass sphere G is indicated at times before $t = 0$ and its shattered fragments F during the explosion are also identified. At later times, shock waves may be seen re-entering the field of view after reflexion from the wall of the shock sphere.

A typical schlieren record of the explosion of a 400 p.s.i. air sphere is shown in figure 11 *a* (plate 4). A schlieren photograph of one of the altitude scaling experiments has also been included for comparison in the above figure. This record, labelled (*b*) in the figure, is one of a 200 p.s.i. air sphere exploded in air at a pressure of 7·3 p.s.i. It has been shown that this explosion should be the same as that of the 400 p.s.i. air sphere case and the records in this figure do, in fact, show very good quantitative agreement. There are, of course, some differences in detail, the slightly later implosion of S_2 in the altitude scaling experiments, for example, but these will be considered at a later stage when the comparison between the theoretical and experimental wave diagrams will be discussed.

Owing to its curvature, the initial glass sphere G is effectively opaque in a

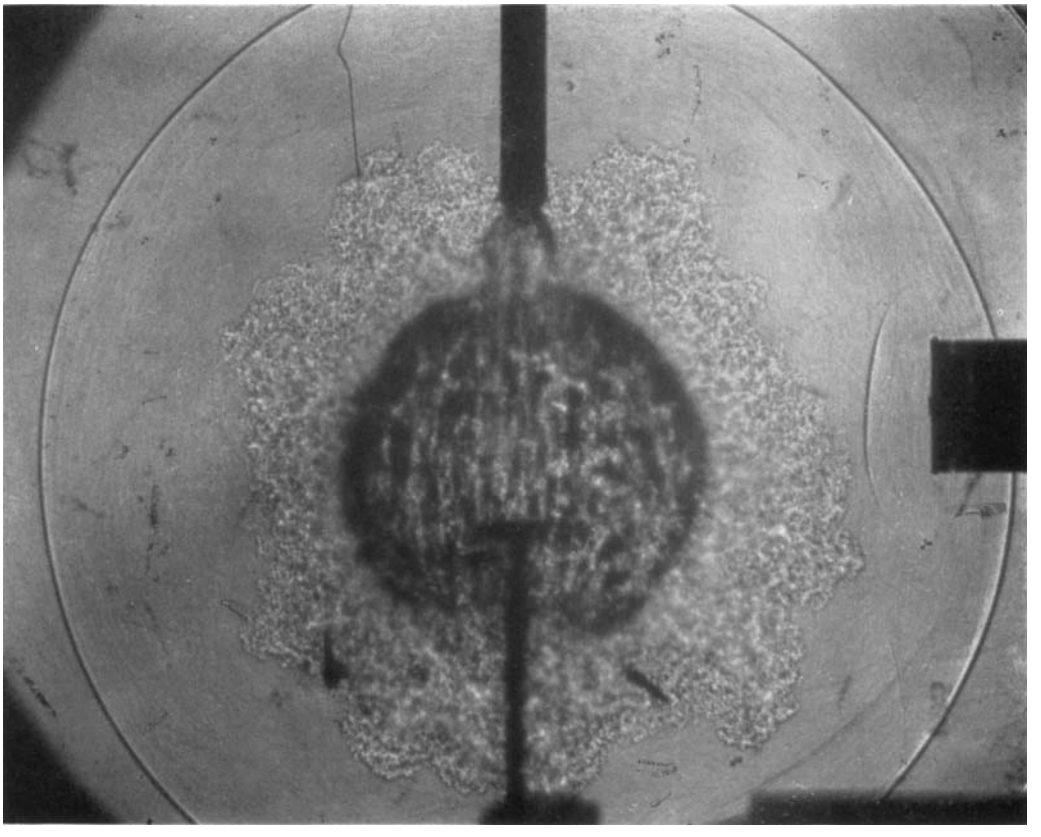

FIGURE 8. Spark shadowgraph of the explosion of a 2 in. diameter sphere of air. SLM pressure gauge mounted at right. Initial sphere pressure = 400 p.s.i. Time delay = 300 μsec.

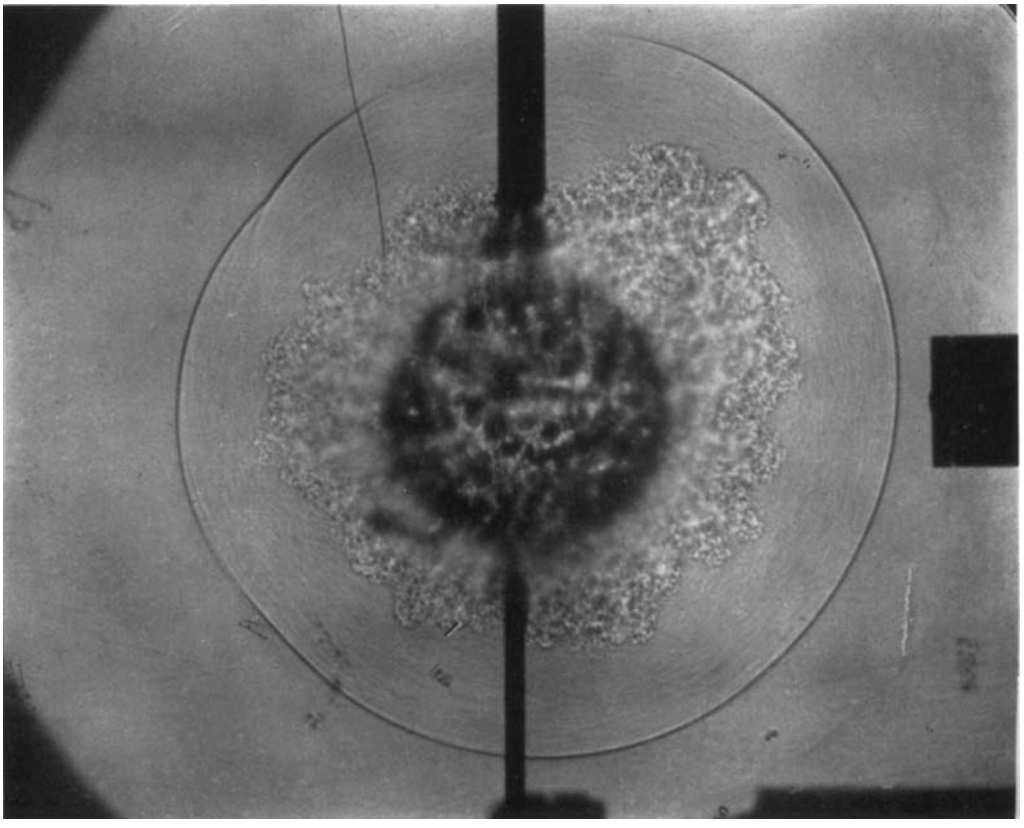

FIGURE 9. Spark shadowgraph of the explosion of a 2 in. diameter sphere of air showing shock reflexion from an SLM pressure gauge. Initial sphere pressure = 400 p.s.i. Time delay = 320 μsec.

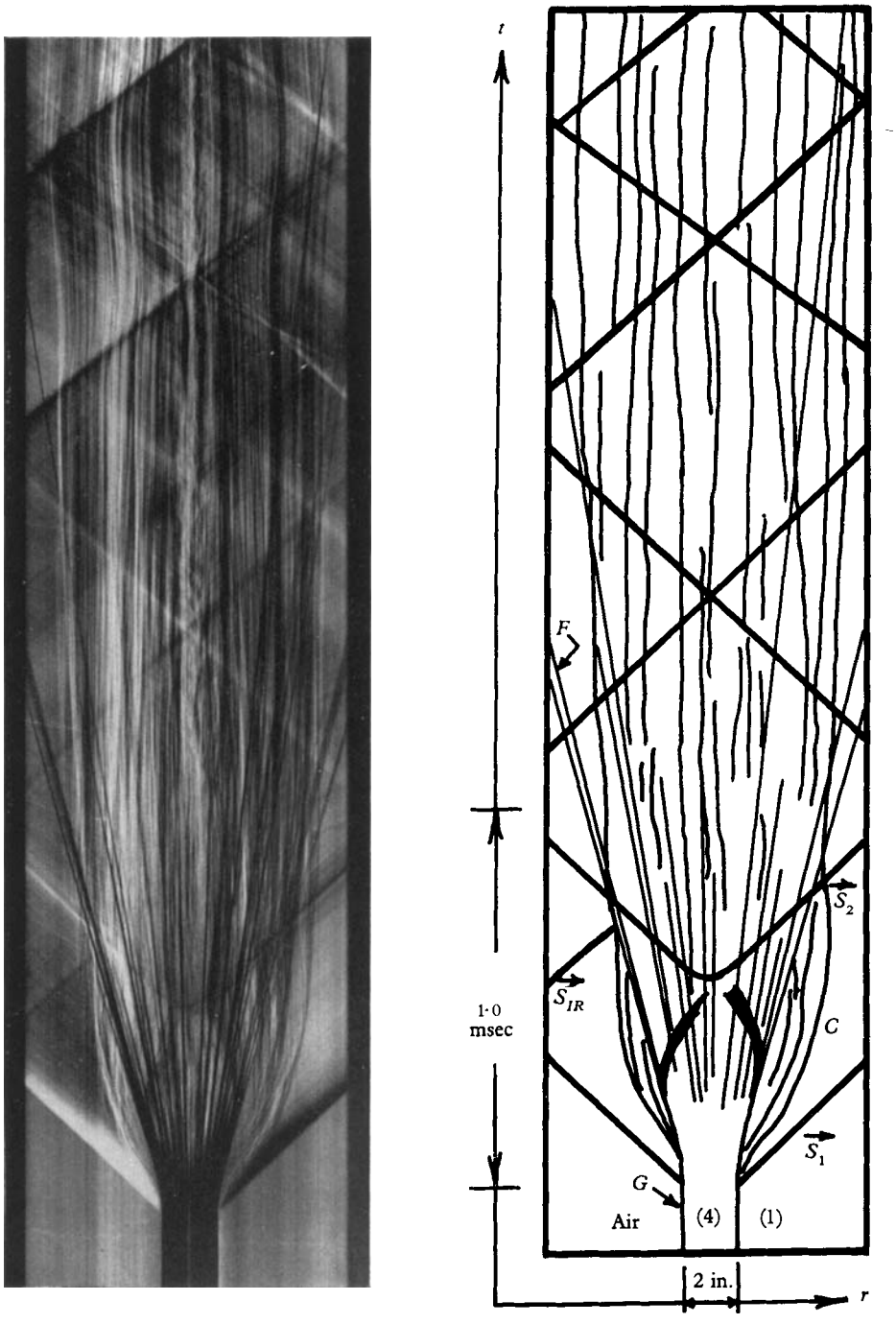

FIGURE 10. Schlieren (r, t)-plane record of the explosion of a 2 in. diameter sphere of air. Explanatory sketch on the right. $p_4 = 326$ p.s.i., $p_1 = 14{\cdot}4$ p.s.i. G = glass sphere still intact; F = fragments of shattered sphere; $T_{1,4} = 24{\cdot}7$ °C.

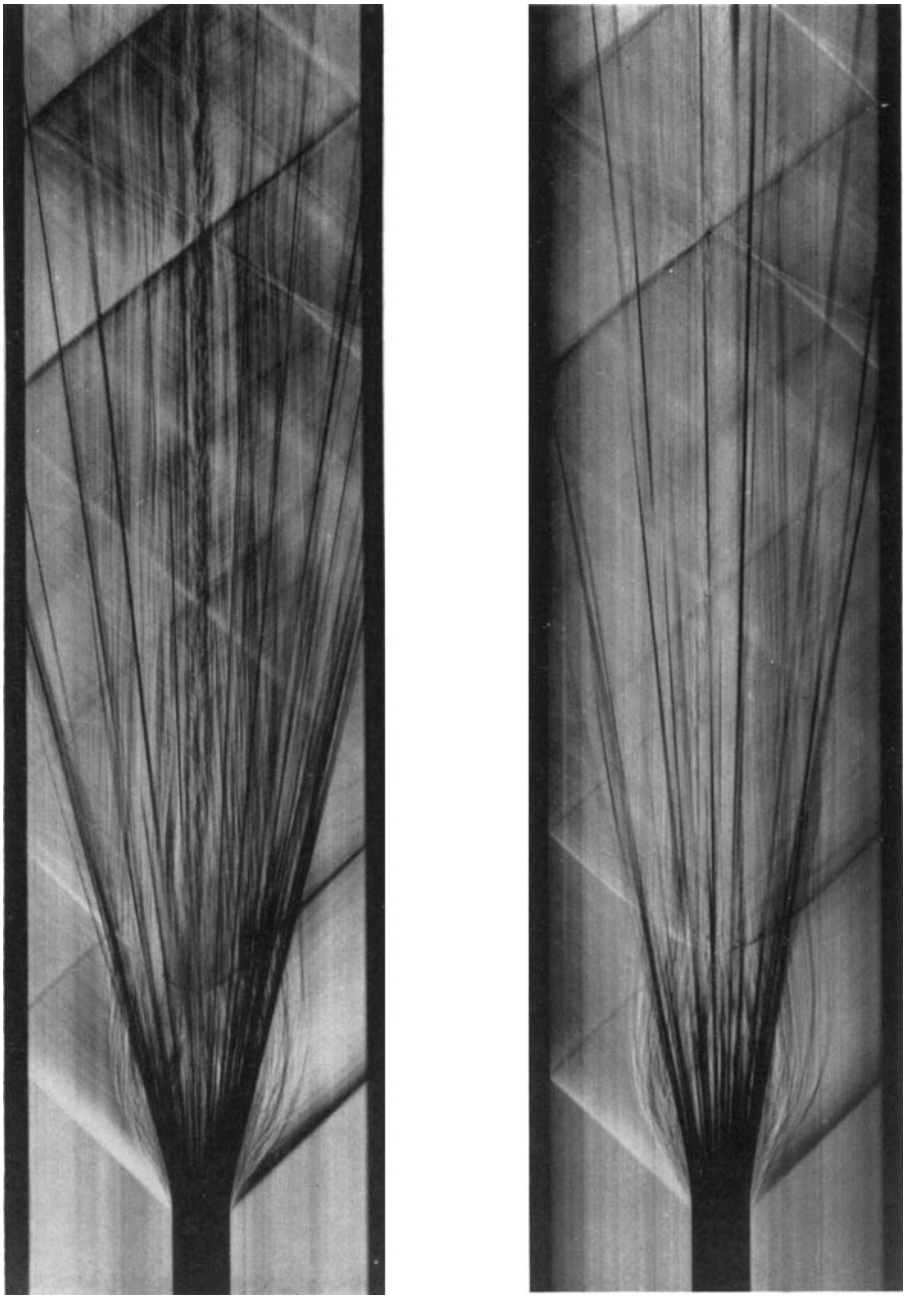

(*a*) (*b*)

FIGURE 11. Schlieren (r, t)-plane records of the explosion of 2 in. diameter spheres of air initially at (*a*) 400 p.s.i. ($p_1 = 14{\cdot}5$ p.s.i.) and (*b*) 200 p.s.i. ($p_1 = 7{\cdot}3$ p.s.i.). $T_{1,1} = 23{\cdot}7$ °C.

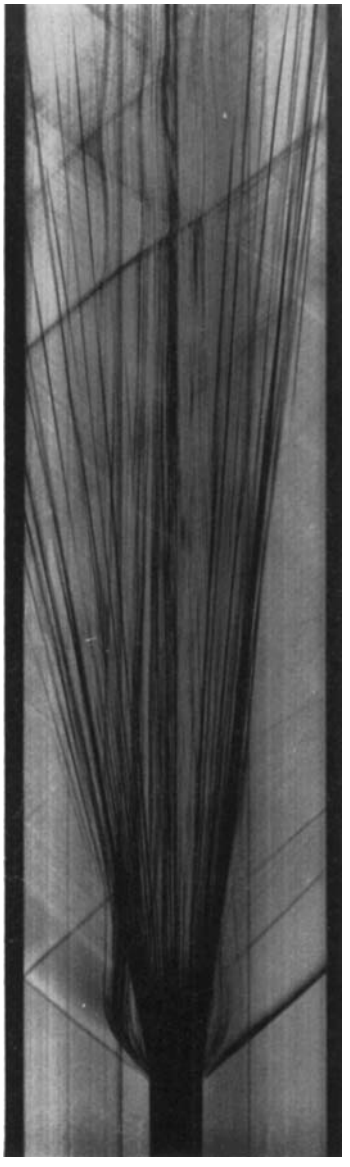

FIGURE 12. Schlieren (r, t)-plane record of the explosion of a 2 in. diameter sphere of helium initially at 326 p.s.i. Shock reflexion from an SLM pressure gauge appears on the left. $p_1 = 14{\cdot}5$ p.s.i. $T_{1,4} = 25{\cdot}5\,^{\circ}\mathrm{C}$.

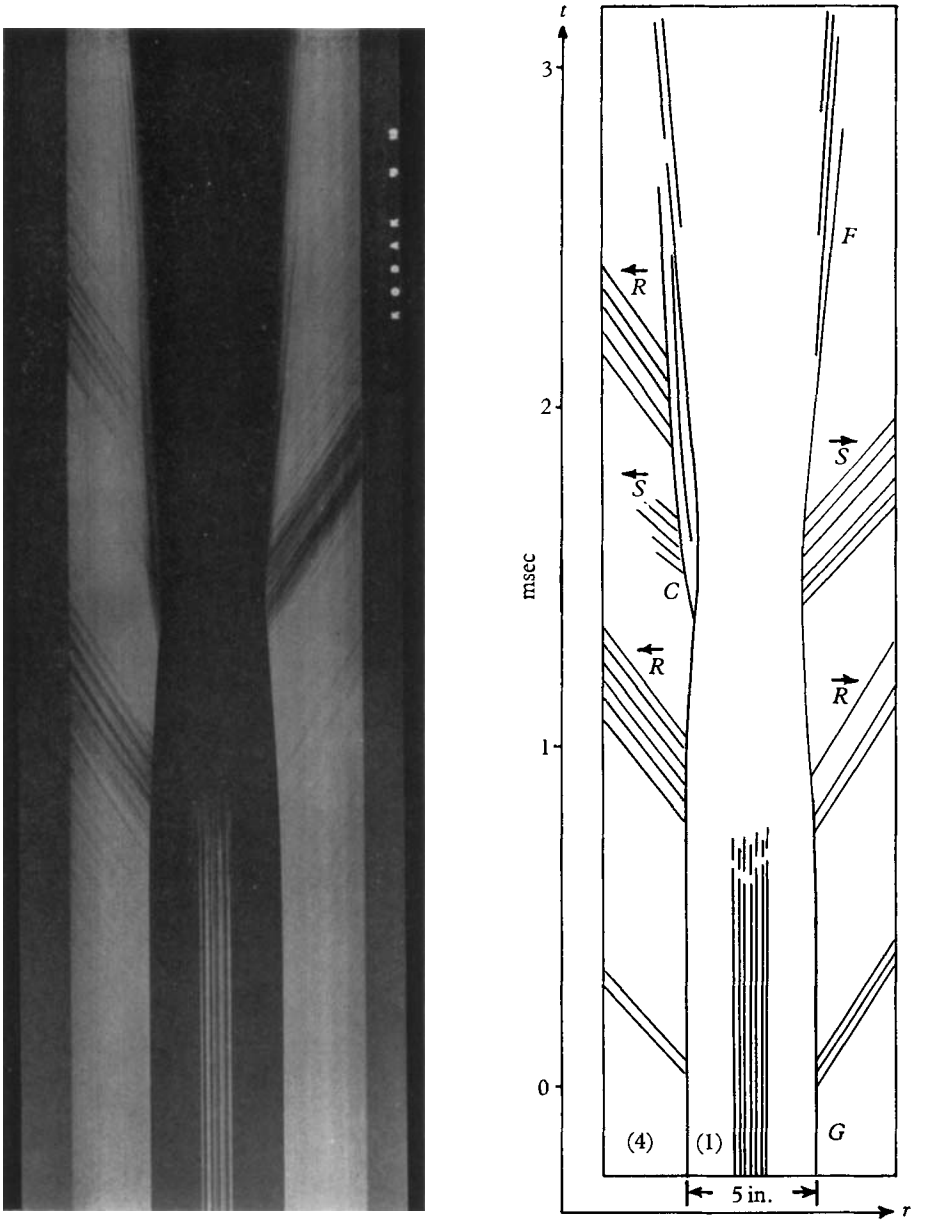

FIGURE 17. Schlieren (r, t)-plane record of the implosion of a 5 in. diameter glass sphere. Explanatory sketch on the right. G = glass sphere still intact. F = fragments of shattered sphere. $p_4 = 65$ p.s.i. (30 % SF_6, 70 % air). $p_1 = 300$ mm Hg (air). $T_{1,4} = 23{\cdot}5\,^{\circ}C$.

schlieren system and, in addition, any interior wave phenomena are completely obliterated by glass fragments during the first 200 μsec of the flow. It was not possible, therefore, to observe the initial rarefaction wave in these experiments.

The schlieren photographs show that prior to implosion, S_2 appears to be composed of several rather poorly defined shocks (figure 10). Disturbances from the shattering glass sphere and the diffraction of the second shock wave around glass fragments during its early growth probably introduce considerable irregularity into the profile of this shock wave. The irregularities in a horizontal plane at right angles to the optical path would then give the appearance of multiple shocks in a schlieren photograph. Furthermore, once formed, the irregularities in the shock profile will not necessarily be damped out as the shock implodes on the sphere centre.

Perry & Kantrowitz (1951) have referred to stable shock waves as those which tend to dampen out random disturbances and assume a profile of uniform curvature. Such stability of form is shown, for example, by all one-dimensional plane, cylindrical and spherical shock waves moving away from their point of origin. The shock stability in the spherical case is well illustrated in the spark shadowgraph pictures. However, in a study on the production of converging (imploding) cylindrical shock waves (Perry & Kantrowitz 1951) it was shown that although a stable convergence may exist for low shock strengths, shock stability decreases with increasing shock strength. This has also been shown to be true in the spherical case (Butler 1956). Similar effects may therefore be expected in the present spherical problems as the second shock wave increases in strength during implosion. However, the present problems are further complicated by the fact that the second shock wave implodes into a non-uniform region and shock profile irregularities may therefore be accentuated by disturbances originating in front of the shock.

The initial diffuseness of the main shock front in the schlieren photographs, and the broad region immediately behind the front, indicate the process of shock formation which has already been pointed out in the spark shadowgraph pictures. The schlieren records show the shock wave to be formed after about 200 μsec, and to have achieved its maximum velocity at this time. A region of expansion associated with the deceleration of the contact front can then be seen following the main shock wave in all the schlieren photographs.

A schlieren photograph of the explosion of a 2 in. diameter sphere of helium initially at 326 p.s.i. is shown in figure 12 (plate 5). The sphere was exploded in air at atmospheric pressure. The record shows good quantitative agreement with the theoretical wave diagram of figure 3. Because of the considerable irregularity in the profile of the contact front, as shown in the shadowgraph pictures, the front appears to have several extremities in the schlieren photograph very much like the case of the imploding shock wave discussed earlier.

A third shock wave is seen moving out behind S_2 and, as indicated in figure 3, it is moving at a higher velocity than the second shock wave. Similarly, S_2 travels at a lower velocity than the main shock wave, in agreement with the theoretical predictions. The third shock wave is not very distinct on the left side of the schlieren record in figure 12, and in fact on many schlieren photographs it could

not be seen at all. However, since this shock wave is generated by the interaction between the second shock wave and the contact surface, the extended and irregular nature of the latter would probably result in the third shock wave being poorly formed and consequently more difficult to detect. The generation of a well-formed fourth shock wave is therefore even less likely. Again, unfortunately, the glass fragments have obliterated the early interior flow and no shock implosion phenomena can be seen.

6.3. *Dimensional scaling*

In view of the fact that the definition of the interior flow in the helium spheres was quite poor, several additional experiments were performed under circumstances such that schlieren records of these explosions represented an effective enlargement of the previous schlieren photographs by a factor of two. In this way it was hoped that something of the interior wave phenomena in the helium-sphere explosions could be observed.

Referring again to the expression for ϵ (equations (3) and (4)), it is seen that for a constant initial pressure ratio, we may write simply that $\epsilon = \text{const.} r_i$. If then similar helium-sphere explosions were generated using 4 in. diameter spheres at the same initial pressure ratio as in the 2 in. diameter cases, the theoretical solutions are still applicable except that the parameters τ and λ now represent times ($t = \epsilon\tau/a_0$) and radial distances ($r = \epsilon\lambda$) which are twice those in the 2 in. diameter sphere problem. This is actually an example of the type of scaling law that may be used in predicting the magnitudes of the blast phenomena associated with the detonation of large solid explosive charges from field and laboratory measurements made on smaller charges (Schardin 1954). Such scaling laws are based on the fact that the properties of a blast wave are unchanged if the scales of length and time by which they are measured, are changed by the same factor as the dimensions of the charge.

Although such laws are strictly applicable only after the shock wave has travelled a certain distance from the source of the explosion, several helium-sphere explosion experiments were performed using 4 in. diameter glass spheres under the same initial pressure ratios as in the ordinary 2 in. helium-sphere cases. Schlieren photographs of these explosions should therefore afford a reasonable check on dimensional scaling in addition to their main purpose of enlarging the flow field in an attempt to observe implosion phenomena.

Unfortunately, no implosion phenomena could be seen in schlieren records of the larger sphere explosions in spite of the fact that the glass fragments did not entirely obliterate the interior region. It is likely, however, that the second shock wave was too poorly formed to be detectable through the turbulent gas of the contact front; it was, in fact, only detectable after it emerged from the contact front. From the point of view of scaling, however, a comparison of the schlieren records of the 2 and 4 in. diameter helium-sphere explosions indicated that the scale of the latter explosions, in distance and time, was approximately doubled over that of the 2 in. diameter sphere cases. As a consequence of scaling, the shock speed (or strength) at a particular radial distance from the 4 in. diameter sphere explosion should be equal to the shock speed at half this radius from the

2 in. diameter sphere explosion. This was found to be approximately the case. The average velocity of the main spherical shock wave between 4 and 5 in. from the 2 in. diameter He/Air case was 1310 ft./sec and that between 8 and 10 in. from the 4 in. diameter He/Air case was 1370 ft./sec.

6.4. *Comparison with theoretical predictions*

The experimental wave systems from all the schlieren records of the 400 p.s.i. air-sphere explosions have been compared with the numerically calculated wave diagram for the Air/Air case. A typical comparison is shown in figure 13. In the interests of clarity, the experimental profiles shown in each of these figures have been chosen as representative of a large group of experimental curves. A typical wave diagram from some of the schlieren photographs of the Air/Air altitude scaling experiments has also been included and is shown by the dashed profile in this figure.

The experimental wave systems are in good agreement with theory in that they exhibit all the main features that were predicated and are modified only by the physical limitations of the glass diaphragm. The figure shows that initially, in the experimental case, the main spherical shock waves travel with a velocity lower than the theoretical value but that after a short time, corresponding to about 4 in. of shock travel, both the theoretical and experimental shock waves move at about the same speed. Immediately after release, the theoretical shock wave attains the velocity prescribed by the initial pressure ratio and then undergoes a rather rapid initial decay. The experimental shock waves, on the other hand, undergo a formation process, as in the plane case, and take a finite time to develop. Furthermore, owing to the inherent radial decay during the formation period, the shocks when formed are considerably weaker than predicted theoretically. Thus although the experimental and theoretical shock waves attain approximately the same speed after about 4 in. of travel, initially the theoretical shock wave races ahead of the compression waves forming the actual shocks.

The experimental second shock waves are in very good agreement with the theory in regard to shock velocity and time of arrival at radii beyond 3 in., in spite of the later implosion times of the second shock waves in practice, times which are of the order to 500 μsec compared with the theoretical implosion time of 350 μsec. The second shock waves implode with a lower velocity and are therefore weaker than theory, most probably as a result of poor formation and non-uniform convergence due to the effects of disturbances produced during the shattering of the glass spheres and the diffraction of these shock waves around glass fragments during their early motion. After implosion, on the other hand, these shock waves reflect with a higher velocity than the computed values. This in turn is probably the result of their lower implosion strengths in that the inward moving, or opposing flow velocities are less than the computed values. The net result is that the motions of the second shock waves in these experiments match the theory to fair accuracy at radii beyond the contact surface.

The contact fronts in the exploding spheres show a marked difference from their theoretical behaviour by expanding to larger radii and exhibiting only very slight oscillation. However, the apparent maximum radii of the contact

surfaces in this figure is artificial. It has already been pointed out that the extremely irregular nature of the contact front causes it to have several apparent extremities in a schlieren photograph. The experimental contact fronts shown in this figure are those traced from the maximum outline of the front in the

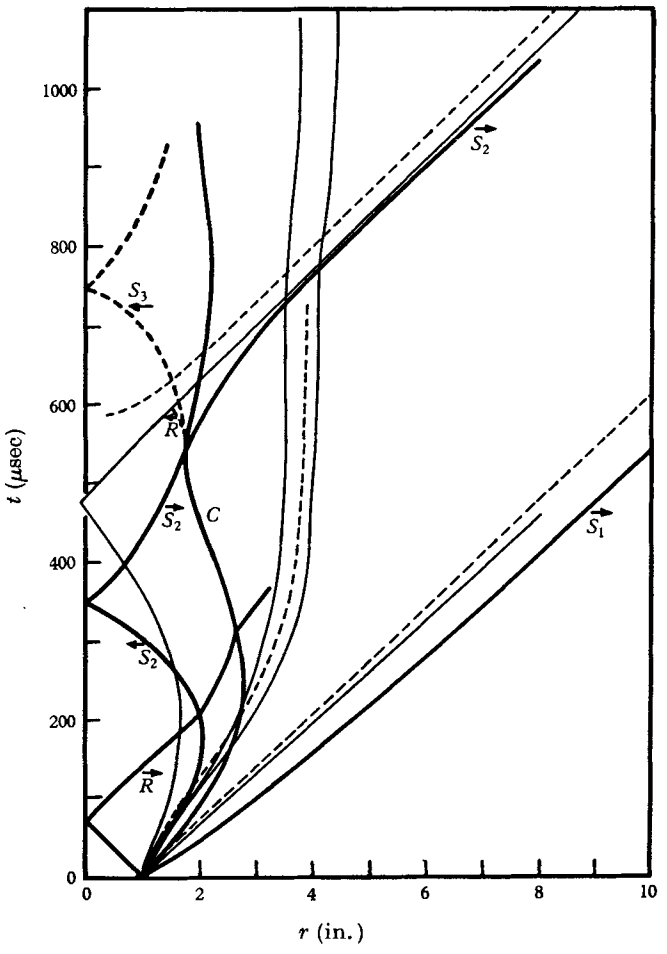

FIGURE 13. Theoretical and experimental wave systems following the shattering of a 2 in. diameter glass sphere initially pressurized with air at room temperature. Theory (initial sphere pressure = 326 p.s.i.), ——; experiment (p_4 = 400 p.s.i., p_1 = 1 atm), ——; experiment (altitude scaling, p_4 = 200 p.s.i., p_1 = 7·3 p.s.i.), – – – –.

photographs and are therefore representative of the maximum radii reached by the gas protuberances in the irregular interface. It is reasonable to say that averaged contact front diameters, i.e. ones that smoothed out the irregularities in profile, would be smaller than those indicated in the figure.

The altitude scaling experiments (200 p.s.i./7·3 p.s.i.) are seen to agree quite well with the experimental wave diagrams from the 400 p.s.i. spheres in figure 13, particularly in the motions of the main spherical shock wave and the contact surface. The times of implosion of the second shock waves, however, are about

60 μsec later than in the 400 p.s.i. sphere explosions, and as a result they tend to arrive at particular radii at slightly later times than the second shock waves of the 400 p.s.i. case, though with approximately the same velocity. The later implosion times are probably the result of a slower breaking process because of the smaller pressure differential across the glass sphere. Because of their initial

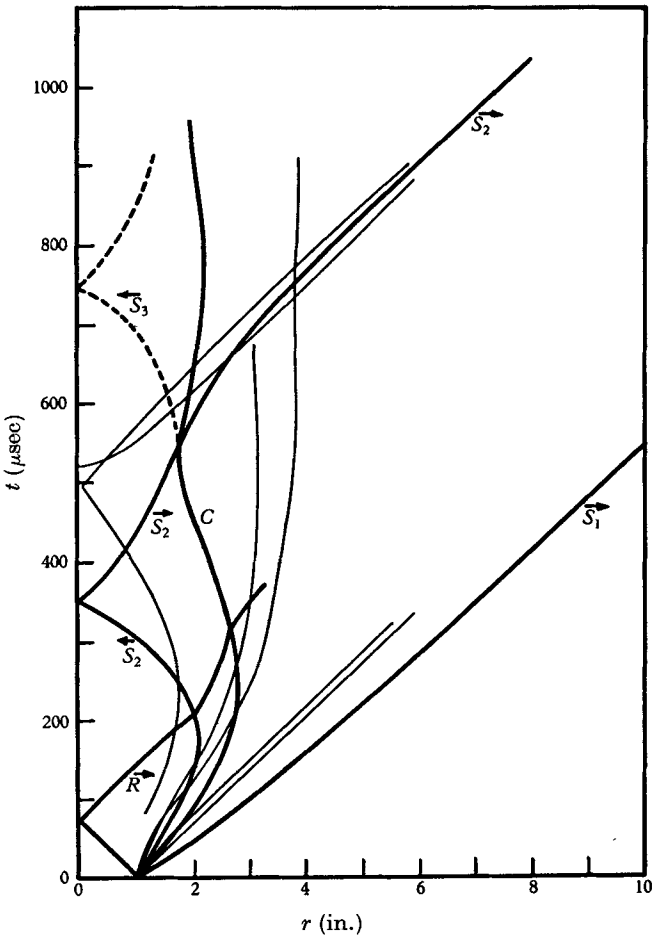

FIGURE 14. Theoretical and experimental wave systems following the shattering of a 2 in. diameter glass sphere initially pressurized to 326 p.s.i. with air at room temperature. Theory, ——; experiment (p_1 = 1 atm), ——.

diffuseness, it was difficult to measure the main shock velocities at times earlier than about 150 μsec. Nevertheless, it has already been shown in figure 13 that velocities during the early shock formation process are considerably less than theoretical values. After formation, however, all the main shock velocities are within 65 ft./sec of the theoretical speed and approach this speed more closely at larger radii.

A comparison between the theoretical wave diagram and the experimental wave systems from the explosion of air spheres, initially at 326 p.s.i., is shown in figure 14. Since the initial sphere pressure in these experiments was that assumed

in the numerical calculations, these explosions therefore incorporated no correction for the kinetic energy of the moving glass fragments. It is seen, however, that the experimental wave systems of figure 14 differ only slightly from those in figure 13. Furthermore, the average shock velocity at a radius of 6 in. from the 326 p.s.i. sphere explosions is only 20 ft./sec less than the shock speed at the same radius in the 400 p.s.i. case, in spite of the fact that an allowance for the motion of the glass fragments was included in the latter experiments.

It is difficult to say whether or not this slight difference in shock speed is reasonable. The results indicate that the correction for the moving glass fragments has had only a very slight effect on the flow, in spite of the fact that the energy added in the pressure corrections accounted for the kinetic energy of the glass to within 3 % in all cases. From this it would appear that the present explosion experiments are not particularly sensitive to initial pressure ratio (p_4/p_1) since, in the air case, for example, a 75 p.s.i. increase in the initial sphere pressure resulted in only a small change in the mean shock velocity. It should not be construed, however, that the correction for the energy of the glass fragments is not effective. It is possible that the correction affects the flow at very early times but that its effect is masked by formation processes. On the other hand, there is the possibility that the smallness of the effect of the pressure correction may be real in that a similar numerical calculation assuming an initial pressure of 400 p.s.i. may exhibit only a small change in the characteristics of the flow.

Experimental wave systems representative of the schlieren records of the 326 p.s.i. helium-sphere explosions are compared with the theoretical wave diagram for the He/Air case in figure 15. A profile representing the results of the He/Air altitude scaling experiments (163 p.s.i./7·3 p.s.i.) has also been included and is indicated by the dashed lines. As in the Air/Air case, the formation process of the main shock waves in practice results in initial velocities which are lower than the theoretical shock velocity. After about 150 μsec, however, the shock waves travel at approximately the theoretical velocity. The contact fronts move out to radii larger than the theoretical radius and then remain essentially stationary. A factor influencing the apparent motion of the contact surface has already been mentioned in the discussion on the air-sphere explosions, and a similar argument applies to the discrepancy between theory and experiment for the helium–air interface.

The second shock waves, at the radii where they are first discernible, arrive about 75 μsec later than the theoretical second shock wave but travel faster, and attenuate less rapidly. Although no implosion phenomena could be seen, the breaking process is similar to that in the air-sphere explosions and could be expected to affect the implosion of the second shock wave in the manner discussed previously for the air case. However, in view of the more rapid implosion and reflexion of the second shock wave in the helium case, the effects of the finite breaking time of the sphere could result in greater time delays between the theoretical and experimental second shock positions in this case.

It has been mentioned previously that because of the extreme irregularity of the interface, the third shock waves were poorly formed and therefore poorly

defined on the schlieren records. Their profiles in figure 15 show considerable variation both in velocity and time of arrival at particular radii. The later arrival of the third shock wave is expected for two reasons. First, the implosion of the second shock wave is late, and secondly, since S_3 is generated by the reflexion of S_2 at the helium–air interface, the larger radius of this interface results in a later second shock-interface interaction and consequently a later S_3

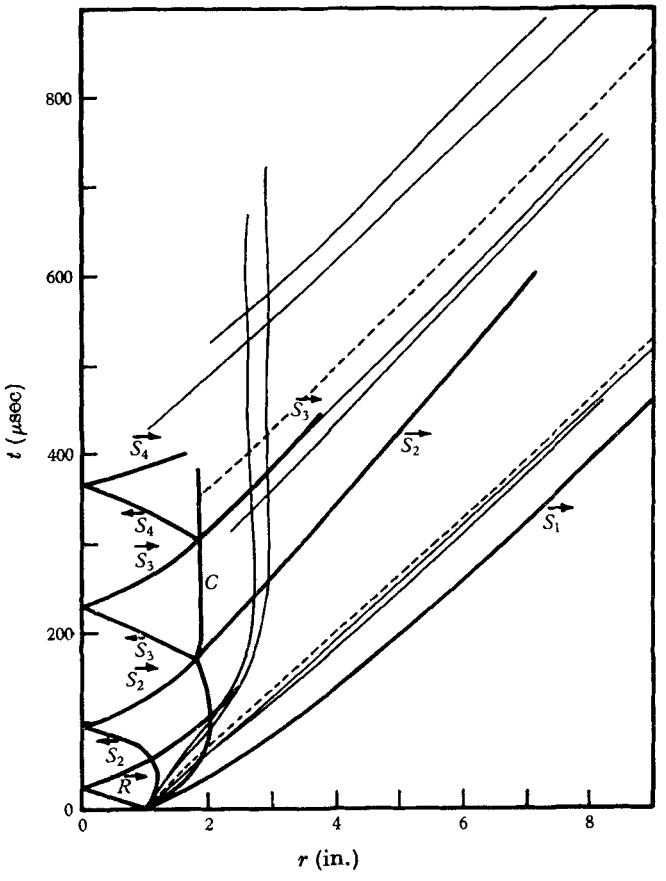

FIGURE 15. Theoretical and experimental wave systems following the shattering of a 2 in. diameter glass sphere initially pressurized with helium at room temperature. Theory (initial sphere pressure = 264 p.s.i.), ——; experiment (p_4 = 326 p.s.i., p_1 = 1 atm), ——; experiment (altitude scaling, p_4 = 163 p.s.i.; p_1 = 7·3 p.s.i.), – – – –.

implosion and reflexion. The results of the altitude scaling experiments show good agreement with the 326 p.s.i. helium-sphere explosions except for the tendency of the second shock waves to arrive at slightly later times than those of the 326 p.s.i. experiments, again indicating a longer formation time when the initial pressure differential is smaller. The same was true in the air sphere altitude-scaling experiments. The velocity of the main shock wave approaches the theoretical velocity more closely as the shock radius increases and is within 15 ft./sec of the theoretical speed at a radius of 8 in.

6.5. *Pressure records*

A typical oscilloscope record of the response of the SLM pressure transducer is shown in figure 16. The trace represents the pressure variation behind the reflected spherical shock wave at a radius of 5·7 in. during the explosion of a 400 p.s.i. air sphere. The arrival of the first and second shock waves at the pressure gauge is clearly seen in this figure. Excellent repeatability was exhibited in the several pressure records obtained at each radial position of the gauge in all experiments.

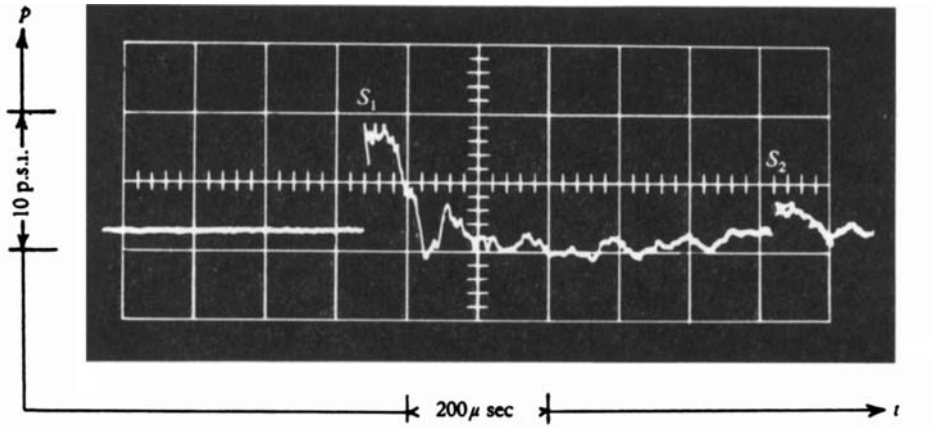

FIGURE 16. Oscilloscope record of the response of an SLM pressure gauge to the blast from a 2 in. diameter sphere of air initially at 400 p.s.i. Gauge face is normal to the flow at a radius of 5·7 in. $p_1 = 14{\cdot}5$ p.s.i. $T_{1,4} = 23{\cdot}5\,^{\circ}\mathrm{C}$.

The results of the pressure measurements are summarized in table 1. The table shows the peak reflected shock overpressures ($\Delta P_R = p_5 - p_1$), measured from the pressure records of the air and helium-sphere explosions, for several radial positions of the pressure gauge. p_5 is the peak reflected shock pressure and p_1 the initial pressure. The measured ΔP_R are compared with the ΔP_R calculated from the velocity w_1 of the main shock wave incident on the pressure gauge. The pressures are shown also in terms of the peak reflected shock-pressure ratio ($P_{51} = p_5/p_1$). The results are in quite reasonable agreement particularly in view of the limitations on the accuracy of the measurement of the shock velocity from the schlieren records and the measurement of the peak ΔP_R from the pressure records.

The shock velocities were determined from the (r, t)-schlieren records by measuring the film velocity (rotational speed of drum camera) and the angle made by the trace of the shock wave with the time direction of the film. The accuracy of shock-velocity measurement was about ± 20 ft./sec (or 1·6 %) at the present shock speeds. However, it may be shown that a variation of 20 ft./sec in the incident shock velocity causes a calculated change of about 1·5 p.s.i. in ΔP_R, or half this value in the altitude-scaling experiments (see columns 6 and 7, table 1). It can further be shown that for the present range of shock strengths, a 1·6 % change in shock velocity produces a 6 % change in reflected shock-pressure ratio (P_{51}).

ΔP_R (p.s.i.) [numerical solution]		
Radius	Air/Air	He/Air
5·7	14·6	12·5
8·0	8·2	7·0
10·0	6·8	5·5

TABLE 1. Peak reflected shock overpressures at selected radii in the explosion of 2 in. diameter glass spheres initially pressurized with air or helium at room temperature.

Pressure record	Case	Initial glass sphere pressure p_4 (p.s.i.)	Initial shock sphere pressure p_1 (mm Hg)	Radial position pressure gauge r (in.)	Shock velocity incident on gauge w_1 (ft./sec)	Peak reflected shock over-pressure calculated from w_1 ΔP_R (p.s.i.)	Measured peak reflected shock over-pressure ΔP_R (p.s.i.)	Incident shock velocity calculated from measured ΔP_R (ft./sec)	Reflected shock pressure ratio (P_{51}) from measured ΔP_R	Reflected shock pressure ratio (P_{51}) from calculated ΔP_R	Reflected shock velocity calculated from w_1 (ft./sec)	Reflected shock velocity measured from (r, t)-records (ft./sec)
P59	Air/Air	400	752	5·7	1240	7·3	7·2	1239	1·50	1·50	1104	1075
P60			754	5·7	1222	5·9	6·3	1227	1·43	1·41	1107	1084
P61			754	5·6	1238	7·1	6·7	1232	1·46	1·49	1104	1087
P76			752	8·0	1222	5·9	4·8	1206	1·33	1·41	1107	1123
P83			748	8·0	1219	5·7	4·4	1201	1·31	1·40	1108	1119
P82			748	10·0	1191	3·7	3·5	1187	1·24	1·26	1116	1137
P62	Air/Air	200	759	5·8	1222	3·0	2·7	1215	1·37	1·41	1107	1091
P64			756	5·7	1217	2·8	2·8	1217	1·38	1·38	1114	1098
P77			752	10·0	1185	1·7	1·7	1186	1·23	1·23	1117	1123
P48	Air/Air	326	745	5·8	1232	6·6	5·6	1217	1·39	1·46	1105	1101
P49			745	5·7	1233	6·7	6·5	1230	1·45	1·47	1105	1075
P50			745	5·7	1227	6·3	6·0	1223	1·42	1·44	1107	1079
P53	He/Air	326	750	5·7	1260	8·9	7·3	1240	1·51	1·62	1099	1123
P54			750	5·7	1277	10·3	8·6	1257	1·60	1·71	1096	1112
P55			750	5·7	1264	9·2	7·3	1240	1·51	1·64	1099	1106
P70			742	8·0	1245	7·6	5·0	1209	1·35	1·53	1102	1101
P71			742	8·0	1230	6·5	4·2	1198	1·29	1·46	1106	1117
P81			753	10·0	1194	3·9	3·4	1186	1·24	1·27	1114	1088
P56	He/Air	163	750	5·7	1277	5·2	3·5	1237	1·48	1·71	1096	1123
P57			752	5·7	1255	4·3	3·1	1226	1·42	1·59	1100	1104
P58			752	5·7	1248	4·0	3·3	1232	1·45	1·55	1101	1072
P73			752	10·0	1180	1·5	1·5	1180	1·20	1·20	1118	1123

The presence of ringing in the response of the SLM pressure gauge to shock-wave reflexion caused some difficulty in the measurement of the Air/Air and He/Air pressure records. Ringing was also present in the pressure records taken during the dynamic calibration experiments on the SLM gauge. In the shock tube case, however, the region behind the reflected shock wave is one of essentially constant pressure and the magnitude of the reflected shock overpressure, taken as that corresponding to the mean of the ringing, could be determined quite easily. In the pressure records of the explosion experiments, however, it is seen that the reflected shock overpressure decreases with time and it was difficult, therefore, to decide with confidence upon a value for the peak ΔP_R in such cases. This was particularly true for the He/Air pressure records as they exhibit a more rapid fall off in pressure than the Air/Air cases. The numerical solutions have, in fact, shown that the duration of positive overpressure in the helium case is shorter than that in the air case at the same shock radius.

In view of the preceding remarks on experimental measurement, the agreement shown in table 1 between the measured peak reflected shock overpressures and those calculated from incident shock-velocity measurements is quite satisfactory. Shown also in this table are values for the incident shock velocity calculated from the measured ΔP_R. It is seen that, with the exception of some of the He/Air results, all the incident shock velocities calculated from the pressure records are within 20 ft./sec of the velocities measured from the schlieren records.

The corresponding values of the peak reflected shock overpressure obtained from the numerical solutions to the Air/Air and He/Air sphere problems are shown at the bottom of table 1. It is evident that the numerically calculated values of ΔP_R differ considerably from the values measured experimentally. This discrepancy is due to the lower velocity of the shock waves in practice, as shown in the wave diagrams on figures 13 to 15. However, the differences between the experimental and theoretical (numerical solution) ΔP_R are readily accounted for by the increase in ΔP_R of at least 1·5 p.s.i. for each 20 ft./sec increment in shock velocity between the experimental and theoretical values. Finally, as a further check on the reliability of the shock-velocity measurements, the reflected shock velocities were calculated from the measured velocities of the waves incident on the pressure gauge. These calculated velocities are shown in table 1 and are seen to be in very good agreement with the reflected shock velocities measured from the schlieren records.

A characteristic feature in all the pressure records is the abrupt fall off in the pressure profile after about 50 μsec and the rise to a peak again after about 120 μsec, followed by a more gradual decay. It would seem that a more reasonable profile would be obtained by ignoring this 'valley' and bridging it instead by a smoothly falling curve. This abrupt fall off in pressure may be the result of the diffraction of the incident shock wave over the gauge holder (figure 9). Since the pressure behind the reflected shock wave on the front face of the holder is greater than the pressure in the diffracted shock wave on the sides of the holder, a rarefaction wave moves in from the perimeter of the face towards the pressure gauge at its centre in order to reduce the pressure.

Based upon calculations using the measured velocity of the incident shock wave, the average time for the head of the rarefaction wave, travelling at sonic velocity, to sweep in from the edge and reach the pressure gauge is 44 μsec. This compares favourably with 49 μsec as the average of the measured times after shock arrival at which the pressure abruptly falls off in the SLM records. The merit of this view could be investigated by increasing the diameter of the reflecting plane at the gauge so that edge disturbances could not arrive during the period of pressure measurement.

It is possible to estimate the shattering times of the glass spheres in these experiments by comparing the times of arrival of the shock wave at a particular radius in the schlieren and the pressure records. In the schlieren records, times are measured from a $t = 0$ corresponding to the time at which the shock wave appears to leave the glass sphere (figure 10). In the pressure records, however, the main sweep of the oscilloscope is triggered at the instant of contact between the mallet and the aluminium foil on the bottom of the glass sphere. Any difference, therefore, between times of shock arrival measured from the schlieren and pressure records approximately represents the time taken for the glass sphere to absorb the energy of mallet impact and shatter. Such time intervals were between 50–60 μsec in the 400 p.s.i. air and 326 p.s.i. helium-sphere explosions. The corresponding times in the altitude-scaling experiments were slightly longer (60–100 μsec) because of the lower internal pressures and consequent smaller initial loading on the glass spheres in these cases, resulting in a slower breaking process.

6.6. *Initial experiments on spherical implosions*

A number of experiments were performed on the implosion of 5 in. diameter glass spheres initially subjected to an external air pressure of 65 p.s.i. and evacuated internally to a pressure of 300 mm Hg. The mounting was similar to that used for the 2 in. spheres in the explosion experiments and the spheres were shattered by the same breaker unit.

Unfortunately, the implosion experiments were only moderately successful. A real obstacle towards obtaining satisfactory results was the tendency of the glass sphere to shatter locally first, at the region of mallet contact, which allowed the external gas to enter the sphere volume from the base, while the rest of the sphere remained essentially intact for several hundred microseconds. This process was clearly shown in spark shadowgraph pictures of the implosions. The unsatisfactory nature of the shattering process was felt to be largely due to insufficient external pressure on the glass sphere. However, a restriction was placed on the maximum shock-sphere pressure by the limited strength of the laminated glass observation windows. Furthermore, the glass spheres are stronger under the compressive loads of implosion studies than they would be under the tensile loads for explosion experiments at the same pressure differential.

A schlieren (r, t)-record of the implosion of a 5 in. diameter sphere is shown in figure 17 (plate 6), together with an explanatory diagram. In this case, the shock sphere was pressurized to 65 p.s.i. with a mixture of air and sulphur-hexafluoride (70 % air, 30 % SF_6), and the interior was evacuated to 300 mm Hg. The figure shows, qualitatively at least, the expected implosion wave configuration.

A rarefaction wave $\vec{R}$ moves out as the external gas expands into the sphere volume. At the same time a shock wave moves in towards the centre, reflects there and moves out, $\vec{S}$, to eventually overtake the rarefaction wave. Actually, the record shows a region of compression rather than a discrete shock. Additional wave elements will be produced as a result of shock-contact front interactions.

The glass sphere is seen to remain apparently intact for several hundred microseconds after being struck by the mallet at $t = 0$, before the interior is gradually obliterated by the arrival of glass fragments from the base of the sphere. The weak waves seen emanating from the sphere from the instant of mallet contact are partly due to vibration of the glass sphere as was confirmed by the appearance of similar waves in the schlieren record of a glass sphere, under no pressure differential, undergoing impact from the mallet.

The results of the implosion experiments, although disappointing, have at least served to point out some of the experimental difficulties that must be overcome for the satisfactory generation of spherical imposions by means of the present technique. Ideally, in analogy with the explosion case, the external pressure should be reasonably close to the crushing pressure of the glass sphere. However, in the event that external pressures are limited by structural considerations, it may be possible to improve the shattering characteristics of the glass spheres by the use of rapidly cooled, or quenched spheres, since the consequent higher internal stresses may result in a more desirable shattering.

7. Conclusions

Reproducible and symmetrical spherical explosions have been produced by the shattering of 2 in. diameter glass spheres, initially pressurized with air or helium. Radius–time plane schlieren photographs of these explosions have shown good quantitative agreement with the corresponding theoretical wave systems in that they exhibit all the main features that were predicted and are modified only by the physical limitations of the glass diaphragm. The schlieren and spark shadowgraph records have shown that there is a formation process associated with the spherical shock waves in practice, resulting in initial shock velocities which are lower than the theoretical predictions. In addition, the presence of glass fragments in the expanding high-pressure sphere gas is responsible for the introduction of considerable turbulence into the contact region.

The experiments have further shown that the present technique may be used to simulate explosions at arbitrary altitudes, by a suitable scaling of the initial sphere and external gas densities, provided no significant imperfect gas effects occur (as would be the case at very high altitudes when scaling is inapplicable). Schlieren records of the explosion experiments performed in a region of half-atmospheric pressure, under conditions scaled to represent the ordinary air and helium-sphere explosions in air at atmospheric pressure, were in excellent agreement with the schlieren records of these latter cases.

The peak pressures measured from the response of a quartz pressure transducer to the reflexion of the spherical shock wave at various radii, have been compared with the pressures calculated from the measured shock velocity at

corresponding radii. The measured and experimentally derived pressures agree to within the limits imposed by the accuracy of shock-velocity measurement.

Initial experiments on the implosion of 5 in. diameter glass spheres were not very satisfactory because of the failure of the spheres to shatter in a desirable manner while under an external pressure of 65 p.s.i.

The author wishes to express his gratitude to Dr G. N. Patterson for his interest and support during this investigation. The problem was suggested by Dr I. I. Glass whose continued advice and suggestions throughout the course of the work are gratefully acknowledged. The discussions with Dr J. H. deLeeuw at various stages of the work have been most helpful. Special thanks are due to Mr L. E. Heuckroth for his able assistance in conducting many of the experiments.

The research was supported by the Defence Research Board of Canada and the United States Office of Naval Research.

REFERENCES

Boyer, D. W. 1959 Spherical explosions and implosions. *Institute of Aerophysics, UTIA Report*, no. 58.

Boyer, D. W., Brode, H. L., Glass, I. I. & Hall, J. G. 1958 Blast from a pressurized sphere. *Institute of Aerophysics, UTIA Report*, no. 48.

Brode, H. L. 1955*a* *J. Appl. Phys.* **26**, 766.

Brode, H. L. 1955*b* The blast from a sphere of high pressure gas. *Rand Corp. Report*, no. P-582.

Brode, H. L. 1956 Point source explosion in air. *Rand Corp. Report*, no. RM-1824-AEC.

Brode, H. L. 1959 *Phys. Fluids* **2**, p. 217.

Butler, D. S. 1956 The stability of converging spherical and cylindrical shock waves. *A.R.D.E. Report*, no. (B) 18/56.

Goldstine, H. H. & von Neumann, J. 1955 *Comm. Pure Appl. Math.* **8**, 327.

Harris, E. G. 1956 Exact and approximate treatments of the one-dimensional blast wave. *NRL Report*, no. 4858.

Latter, R. 1955 *J. Appl. Phys.* **26**, 954.

Lin, S. C. 1954 *J. Appl. Phys.* **25**, 54.

von Neumann, J. 1944 Shock hydrodynamics and blast waves. *Los Alamos Scientific Laboratory Report*, no. AECD-2860.

von Neumann, J. & Richtmyer, R. D. 1950 *J. Appl. Phys.* **21**, 232.

Perry, R. W. & Kantrowitz, A. 1951 *J. Appl. Phys.* **22**, 878.

Plesset, M. S. 1954 *J. Appl. Phys.* **25**, 96.

Schardin, H. 1954 *Comm. Pure Appl. Math.* **7**, 223.

Taylor, G. I. 1950*a* *Proc. Roy. Soc.* A, **201**, 159.

Taylor, G. I. 1950*b* *Proc. Roy. Soc.* A, **201**, 192.